NEOPLASIA
www.neoplasia.com

Volume 19 Number 4 April 2017 pp. 288–300 288

The Transient Receptor Potential Melastatin 7 Channel Regulates Pancreatic Cancer Cell Invasion through the Hsp90α/uPA/MMP2 pathway[1]

Pierre Rybarczyk*,†,2, Alison Vanlaeys*,†,2, Bertrand Brassart†,‡,2, Isabelle Dhennin-Duthille*,†, Denis Chatelain§, Henri Sevestre*,†,§, Halima Ouadid-Ahidouch*,†,2 and Mathieu Gautier*,†,2

*Laboratoire de Physiologie Cellulaire et Moléculaire-EA4667, UFR Sciences, Université de Picardie Jules Verne, F-80039 Amiens, France; †SFR CAP-Santé (FED 4231); ‡UMR CNRS 7369 Matrice Extracellulaire et Dynamique Cellulaire (MEDyC), Université de Reims Champagne Ardenne (URCA), F-51095 Reims, France; §Service d'anatomie pathologique, CHU d'Amiens, Université de Picardie Jules Verne, F-80000 Amiens, France, France

Abstract

Pancreatic ductal adenocarcinoma (PDAC) is an aggressive malignancy with a very poor prognosis. There is an urgent need to better understand the molecular mechanisms that regulate PDAC cell aggressiveness. The transient receptor potential melastatin 7 (TRPM7) is a nonselective cationic channel that mainly conducts Ca^{2+} and Mg^{2+}. TRPM7 is overexpressed in numerous malignancies including PDAC. In the present study, we used the PANC-1 and MIA PaCa-2 cell lines to specifically assess the role of TRPM7 in cell invasion and matrix metalloproteinase secretion. We show that TRPM7 regulates Mg^{2+} homeostasis and constitutive cation entry in both PDAC cell lines. Moreover, cell invasion is strongly reduced by TRPM7 silencing without affecting the cell viability. Conditioned media were further studied, by gel zymography, to detect matrix metalloproteinase (MMP) secretion in PDAC cells. Our results show that MMP-2, urokinase plasminogen activator (uPA), and heat-shock protein 90α (Hsp90α) secretions are significantly decreased in TRPM7-deficient PDAC cells. Moreover, TRPM7 expression in human PDAC lymph node metastasis is correlated to the channel expression in primary tumor. Taken together, our results show that TRPM7 is involved in PDAC cell invasion through regulation of Hsp90α/uPA/MMP-2 proteolytic axis, confirming that this channel could be a promising biomarker and possibly a target for PDAC metastasis therapy.

Neoplasia (2017) 19, 288–300

Introduction

Pancreatic ductal adenocarcinoma (PDAC) represents more than 80% of all pancreatic cancers. PDAC is the fourth most common cause of global cancer-related death [1]. With 5-year survival rate of less than 5% and a median survival of 6 months after diagnosis, PDAC has the poorest prognosis of all solid cancers. This high mortality is due to the absence of symptoms at early stages without any routine screening test for PDAC. Moreover, there is no specific treatment for PDAC because surgery associated or not with chemo- and radiotherapies only increases 5-year survival to 20%. The majority of patients already have metastases dissemination which is associated with an extremely poor prognosis [2]. Thus, there is an urgent need to find new targets against PDAC metastasis formation

Address all correspondence to: Mathieu Gautier, University of Picardie Jules Verne, F-80039 Amiens, France.
E-mail: mathieu.gautier@u-picardie.fr
[1] P. R. was a recipient of funding from the Ministère de l'Enseignement Supérieur et de la Recherche. A. V. is a recipient of funding from the Conseil Régional de Picardie. This work was supported by FEDER, la Ligue Contre le Cancer (Septentrion), and la SFR CAP-Santé (FED 4231).
[2] Both authors contributed equally to this work.
Received 30 September 2016; Revised 5 January 2017; Accepted 13 January 2017

1476-5586
http://dx.doi.org/10.1016/j.neo.2017.01.004

and dissemination. Metastasis is based on a complex mechanism called the metastatic cascade. Cell invasion including basal membrane degradation and spreading in the surrounding stroma is an important step of the metastatic cascade. Among the proteins that regulate the metastasis cascade, transmembrane ion channels and transporters (called transportome) provide signaling pathways that drive cell invasion [3,4].

Ion channels are integral membrane proteins that are involved in many physiological and pathological processes. There is growing evidence that cancer cell hallmarks are strongly regulated by ion channels including K^+ [5–7], Ca^{2+} [8–10], and Na^+ channels [11,12]. In particular, several channels including transient receptor potential (TRP) channels are implicated in molecular mechanisms of the metastatic cascade [4]. TRPs are nonselective cation channels that are mainly permeable to Ca^{2+}, Mg^{2+}, Na^+, and K^+. Among TRP channels, the transient receptor potential melastatin related 7 (TRPM7) channel is a Ca^{2+}/Mg^{2+} channel fused with a functional kinase domain that belongs to the α-kinase family [13,14]. We and others showed that TRPM7 is involved in migration and/or invasion of epidermal cancer cells including neuroblastoma [15,16], glioblastoma [17], breast cancer [18,19], nasopharynx cancer [20,21], lung cancer [22], prostate cancer [23], and PDAC [24,25]. Importantly, TRPM7 is required for breast cancer metastasis formation in mouse xenograft, and high channel expression is an independent marker of poor outcome in breast cancer patients [26]. Moreover, TRPM7 expression contributes to neuroblastoma progression and metastatic properties by maintaining progenitor-like features [27]. In PDAC, we have shown previously that TRPM7 is overexpressed in human cancer tissues when compared to the healthy ones [24]. Moreover, TRPM7 expression is associated with cancer progression and poor outcome in PDAC. Nevertheless, the molecular mechanisms that regulate PDAC cell invasion are poorly understood. In the present study, we aim to determine how TRPM7 regulates PDAC cell invasiveness.

Results

TRPM7 Expression in PDAC Cell Lines

First, we determined TRPM7 expression in PANC-1 and MIA PaCa-2 PDAC cell lines by reverse transcriptase polymerase chain reaction (RT-PCR) and Western blot (Figure 1). TRPM7 mRNAs (Figure 1*A*) and proteins (Figure 1*B*) are detected in both PDAC cell lines. As TRPM7 is able to form heteroteramers with its close homologue TRPM6, we also assessed TRPM6 expression. TRPM6 mRNA is not detected in the PANC-1 cell line but is found in the MIA PaCa-2 cell line, indicating that TRPM7 is expressed in both PANC-1 and MIA PaCa-2 PDAC cell lines in contrast to the TRPM6 expression which is cell line dependent.

When expressed at the plasma membrane, TRPM7 channels are responsible for the magnesium-inhibited cation (MIC) currents [13,14]. Thus, whole-cell patch clamp was used to study the TRPM7 expression at the plasma membrane and to further characterize MIC currents in PANC-1 cells (Figure 2). MIC currents are recorded after dialyzing intracellular media by an intrapipette solution containing EGTA to chelate intracellular Mg^{2+}. MIC currents develop during the cytosol dialysis and reach a steady state in ~15 minutes (Figure 2*A*, averaged trace of nine cells). These currents have a typical shape of TRPM7-like currents with a small inward component (−2.6±0.9 $pA.pF^{-1}$ at −100 mV), a reversal potential close to 0 mV, and a strong outward rectification (19.5±3.6 $pA.pF^{-1}$ at +100 mV; Figure 2*B*, averaged trace of nine cells). Intracellular Mg^{2+} inhibits MIC currents in a concentration-dependent manner. The free Mg^{2+} concentration in the patch clamp pipette is calculated using the WEBMAX software. MIC currents are inhibited by free $[Mg^{2+}]_i$ of 210 μM, 400 μM, and 680 μM (Figure 2*C*). Although inward currents recorded at −100 mV are not significantly reduced by Mg^{2+} [−2.6±0.9 $pA.pF^{-1}$ for control (n=9), −3.7±0.7 $pA.pF^{-1}$ for 210 μM (n=7), −1.6±0.4 $pA.pF^{-1}$ for 400 μM (n=7), and −0.7±0.6 $pA.pF^{-1}$ for 680 μM (n=6); P=0.062], a strong decrease of outward rectification is induced by intracellular Mg^{2+} (Figure 2, *C* and *D*). Indeed, MIC currents recorded at +100 mV are reduced from 19.5±3.6 $pA.pF^{-1}$ for control (n=9) to 13.2±1.1 $pA.pF^{-1}$ for 210 μM (n=7) and 8.9±1.5 $pA.pF^{-1}$ for 400 μM (n=7) and fully abolished for 680 μM (−0.7±0.6 $pA.pF^{-1}$; n=6; P<0.001). Moreover, TRPM7 is also sensitive to MgATP within a range of free $[Mg^{2+}]_i$ that produces only moderate inhibitory effects on currents [13]. Here, we show that the addition of 1 mM ATP to 210 μM free $[Mg^{2+}]_i$ induced a strong inhibition of MIC currents (3.2±1.8 $pA.pF^{-1}$ at +100 mV; n=3; P<0.05 when compared to the control 0 free $[Mg^{2+}]_i$ and to the 210 μM free $[Mg^{2+}]_i$ alone), suggesting that MIC currents recorded in PANC-1 cells are due to TRPM7 activity (Figure 2, *E* and *F*).

Role of TRPM7 in MIC Current recorded in PDAC Cells

To date, specific pharmacological TRPM7 blockers are not available. Thus, both transient TRPM7 silencing and stable TRPM7 silencing by small interfering RNA (siRNA) or short hairpin RNA (shRNA) are used to confirm that TRPM7 is responsible for the MIC currents recorded at the MIA PaCa-2 and PANC-1 plasma membrane. We previously validated siRNA targeting TRPM7 in human breast and pancreatic cancer cells [19,24,28]. TRPM7

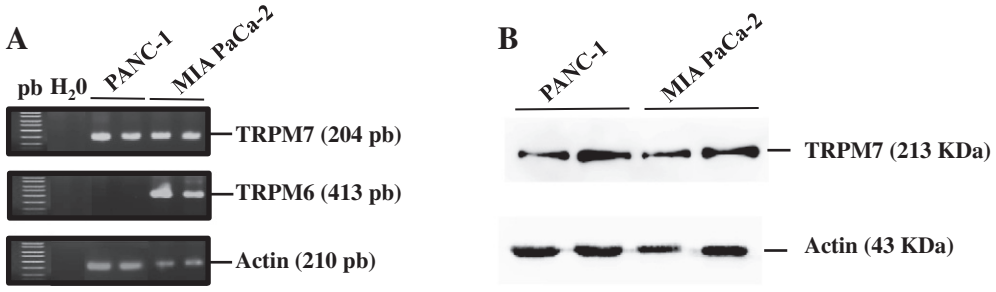

Figure 1. TRPM7 and TRPM6 channel expression in human PDAC cell lines. (A) Both TRPM7 and TRPM6 mRNAs are detected in the MIA PaCa-2 human PDAC cell line by RT-PCR in two different passages, whereas PANC-1 cells express only TRPM7 channel. Water is used as negative control. (B) Western blot indicating that TRPM7 protein is expressed in both PANC-1 and MIA PaCa-2 cell lines.

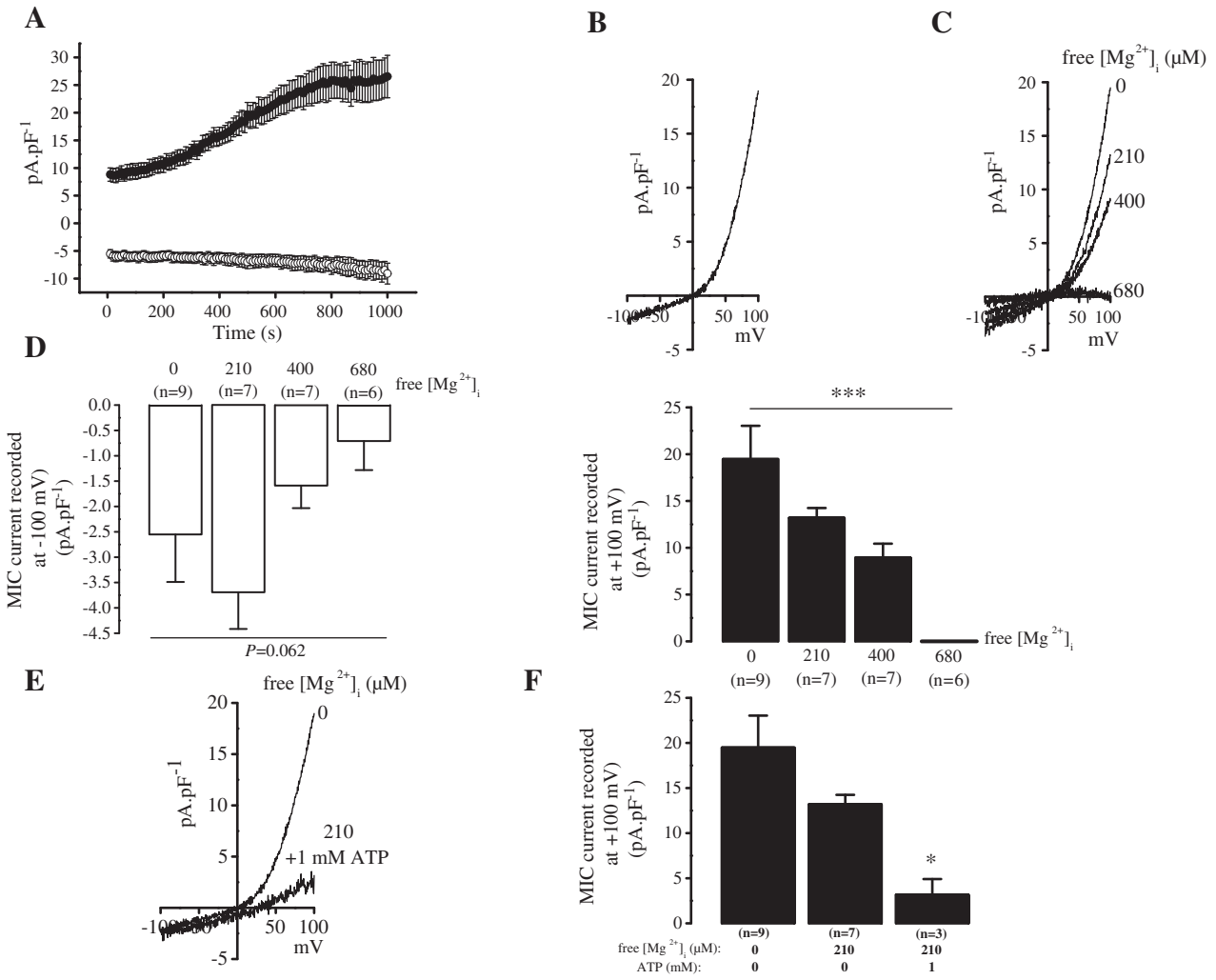

Figure 2. Electrophysiological properties of MIC currents in PANC-1 cells. (A) Membrane currents are recorded after 350-millisecond ramp depolarization from −100 mV to +100 mV at 0.1 Hz under whole-cell patch clamp. MIC currents are activated by dialyzing the intracellular media by an intrapipette solution without Mg^{2+}. Both outward currents recorded at +100 mV (black circles; n=9 cells) and inward currents recorded at −100 mV (white circles; n=9 cells) increase following intracellular Mg^{2+} depletion. (B) Endogenous MIC currents have an inward component, a strong outward rectification, and a membrane reversal potential close to 0 mV (averaged trace of nine recordings). (C) Dialyzing of intracellular media with intrapipette solutions containing Mg^{2+} decreases MIC currents in a dose-dependent manner. (D) MIC currents recorded at −100 mV (white histograms) and at +100 mV (black histograms) are inhibited by increasing intracellular free Mg^{2+} from 0 (n=9 cells) to 210 (n=7 cells), 400 (n=7 cells), and 680 μM (n=6 cells). (E) Addition of 1 mM ATP in the intrapipette solution potentiates the inhibitory effect of Mg^{2+} on MIC currents (n=3 cells). (F) Interacting effects of intracellular free Mg^{2+} and ATP on outward MIC currents recorded at +100 mV. MIC currents are inhibited by 1 mM ATP complexed with 210 μM free Mg^{2+} (n=3 cells) when compared to 210 μM free Mg^{2+} (n=7 cells) and to 0 free Mg^{2+} (n=9 cells).

silencing with shRNA or siRNA induces a TRPM7 mRNA decrease of 62±3% (Figure 3*A*; N=3; P<0.001) and 67±15% (Figure 3*D*; N=3; P<0.05) in PANC-1 and MIA PaCa-2 cells, respectively, when normalized to the control condition. As shown in Figure 3, MIC currents recorded at +100 mV are reduced from 29.6±4.6 pA.pF^{-1} (n=6) to 5.0±2.4 pA.pF^{-1} (n=4; P<0.001; Figure 3, *B* and *C*) in PANC-1 cells stably transfected by shRNA and from 15.7±2.6 pA.pF^{-1} (n=12) to 1.8±1.1 pA.pF^{-1} (n=6; P<0.01; Figure 3, *E*–*F*) in MIA PaCa-2 cells transfected by siRNA.

Role of TRPM7 in Constitutive Cation Entry and Basal Ca^{2+} and Mg^{2+} Homeostasis

TRPM7 channels are permeable for Ca^{2+} [29] and Mg^{2+} [30]. Constitutive cation entry is measured by Mn^{2+} quenching of Fura-2 fluorescence technique (Figure 4). TRPM7 silencing significantly reduces Mn^{2+} quenching slope in both PANC-1 (from –1.73±0.11 to –1.05±0.07; n=166 and 216, respectively; P<0.001; Figure 4*A*) and MIA PaCa-2 cell lines (from –2.16±0.13 to 0.77±0.1; n=171 and n=112, respectively; P<0.001; Figure 4*B*). These experiments indicate that TRPM7 channels constitutively conduct divalent cations entry in PDAC cells. Furthermore, we measure both basal Ca^{2+} and Mg^{2+} intracellular fluorescence using Fura-2 and MagFura-2 probes, respectively, to determine whether TRPM7 channels regulate Ca^{2+} and Mg^{2+} homeostasis in PANC-1 and MIA PaCa-2 cells.

Stable TRPM7 silencing failed to affect Ca^{2+} basal fluorescence (1.05±0.03; n=80) when compared to sh-Control (1.00±0.02; n=59; P>0.05; Figure 5*A*) in PANC-1, whereas we observed a significant decrease of Fura-2 fluorescence in TRPM7-silenced MIA PaCa-2 cells

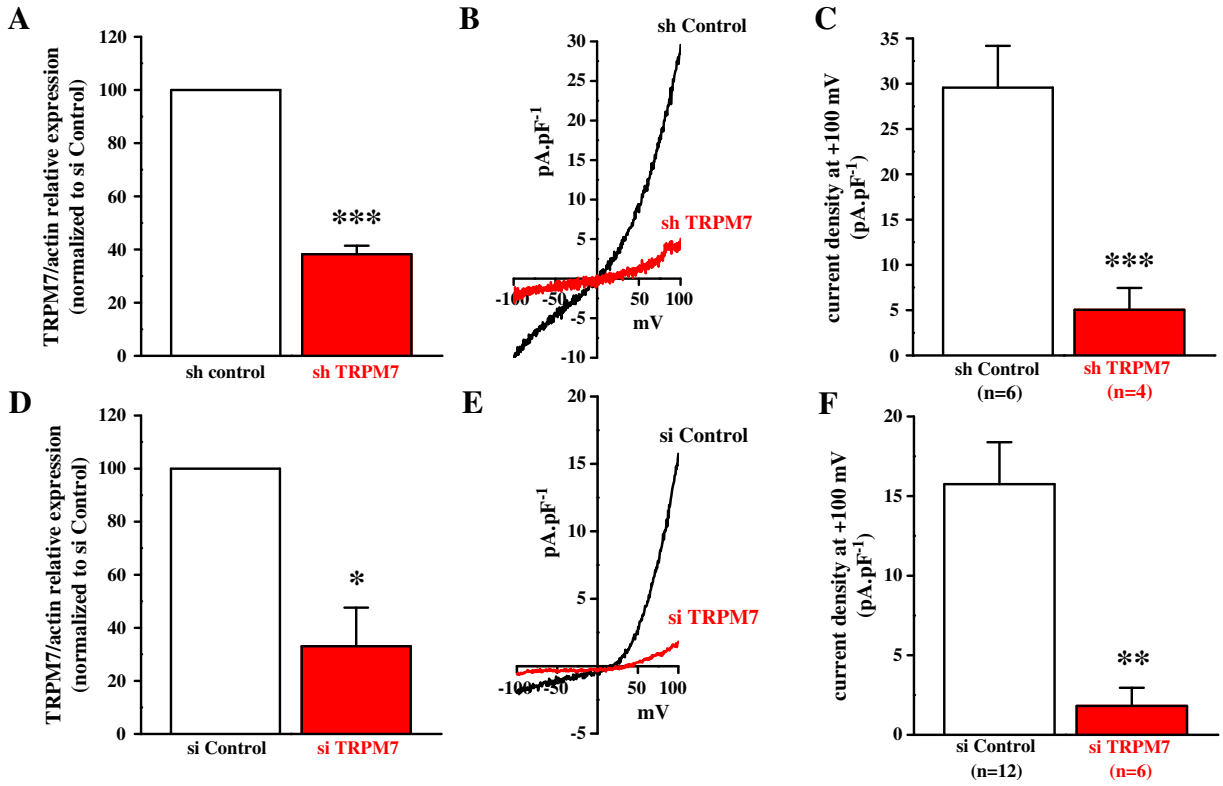

Figure 3. TRPM7 silencing inhibited MIC current in PDAC cells. (A) Effect of TRPM7 silencing by shRNA on TRPM7 mRNA expression in PANC-1 cells (N=3; P<0.001). (B) TRPM7 silencing by shRNA inhibits MIC currents in PANC-1 cells (averaged traces of six recordings for sh-Control and four recordings for sh-TRPM7 conditions). (C) Outward MIC currents recorded at +100 mV are decreased in cells treated with sh-TRPM7 (n=4 cells) when compared to control (n=6 cells; P<0.001). (D) TRPM7 silencing with siRNA decreases mRNA expression in MIA PaCa-2 (N=3; P<0.05). (E) MIC currents were decreased in MIA PaCa-2 cells transfected with siRNA (averaged trace of 6 recordings) when compared to controls (averaged trace of 12 recordings). (F) Outward MIC currents recorded at +100 mV are decreased in cells treated with si-TRPM7 (n=6 cells) when compared to control (n=12 cells; P<0.01).

(1.14±0.01; n=85) when compared to si-Control (1.24±0.02; n=96; P<0.001; Figure 5*B*). These results indicate that TRPM7 regulation of Ca^{2+} homeostasis seems dependent of the cell line.

Stable TRPM7 silencing induces a significant decrease of Mg^{2+} basal fluorescence from 0.67±0.02 in sh-Control (n=110) to 0.61±0.01 in sh-TRPM7 induced in PANC-1 (n=132; P<0.001; Figure 5*C*). Intracellular basal Mg^{2+} level regulation by TRPM7 is also observed in MIA PaCa-2 because TRPM7 silencing decreases MagFura-2 fluorescence from 0.79±0.01 in control (n=105) to 0.74±0.01 in transfected cells (n=105; P<0.01; Figure 5*D*). These data confirm that TRPM7 is mainly involved in Mg^{2+} homeostasis in cancer pancreatic cells.

Role of TRPM7 in PDAC Cell Invasion

TRPM7 channels are involved in cancer cell proliferation, migration, and invasion. It has been shown that TRPM7 reduces chemotaxis-induced invasion in pancreatic cancer cell lines [25]. In this study, we are interested in the role of TRPM7 in PDAC basal cell invasion, without any external stimulation. TRPM7 silencing has no effect on PANC-1 and MIA PaCa-2 cell proliferation measured at 24, 48, and 72 hours (Figure 6*A*). On the other hand, TRPM7 knockdown decreased basal cell invasion by 74.45±1.54% (n=120; N=3) when compared to control (100±4.94%; n=120; N=3; P<0.001) in PANC-1 and by 65.69±2.95% (n=100; N=3) when compared to control (100±6.88%; n=100; N=3; P<0.001; Figure 6*B*) in MIA PaCa-2 cells. The effect of TRPM7 silencing on cancer pancreatic cell invasion cannot be attributed to an effect on cell viability because there is no effect on MTT assays performed at the same time as invasion assays (Figure 6*C*). Taken together, these data suggest that TRPM7 regulates cell invasiveness in PDAC cells.

Role of TRPM7 in the Hsp90α/uPA/MMP-2 Proteolytic Pathway

Cell invasiveness is related to matrix metalloproteinases (MMPs) secretion and extracellular matrix degradation. Thus, we assessed the effect of TRPM7 silencing on protease secretion using gelatin zymography technique (Figure 7). Pro-MMP-2 secretion is decreased by 52±5% in PANC-1 transfected with sh-TRPM7 when compared to sh-Control (N=3; P<0.001; Figure 7, *A* and *B*). Furthermore, TRPM7 silencing also decreased the urokinase-type plasminogen activator (uPA) secretion by 58±9% when compared to sh-Control (N=3; P<0.05; Figure 7, *C* and *D*). Moreover, we also detected the inhibition of the heat-shock protein 90 alpha (Hsp90α) secretion following stable TRPM7 silencing (38±3%; N=3; P<0.01; Figure 7, *E* and *F*). Similar results are found in MIA PaCa-2 cells transfected with siTRPM7. Indeed, TRPM7 silencing inhibited pro-MMP-2 and uPA secretions, respectively, by 27±9% (N=4; P<0.05; Figure 7, *A* and *B*) and 41±1% (N=3; P<0.05; Figure 7, *C* and *D*). Finally, TRPM7 silencing also inhibited Hsp90α secretion by 75±1% (N=4;

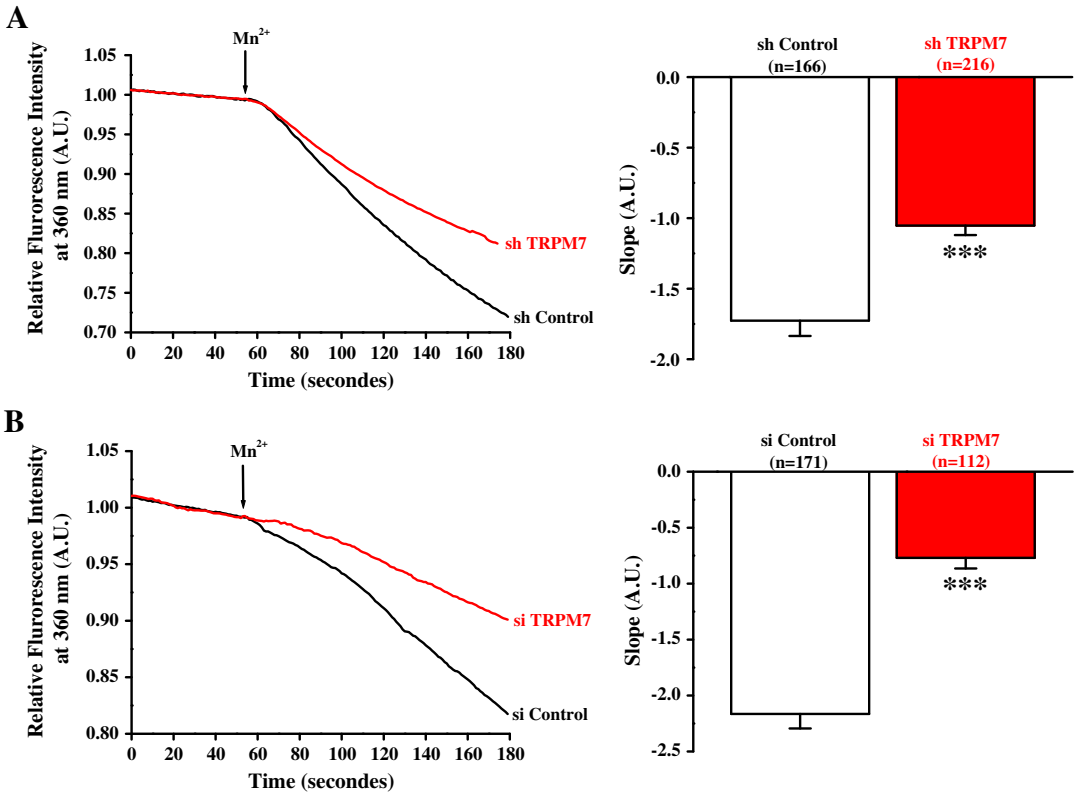

Figure 4. TRPM7 regulated a constitutive divalent cations entry in PDAC cells. (A) TRPM7 silencing induced by shRNA decreases Mn^{2+} quenching of Fura-2 fluorescence in PANC-1 cells (averaged trace of 216 cells) when compared to control (averaged trace of 166 cells), with a significant reduction of quenching slope induced in sh-TRPM7 cells (histograms; $P<0.001$). (B) TRPM7 silencing also reduced Mn^{2+} quenching of Fura-2 fluorescence in MIA PaCa-2 cells (averaged trace of 112 cells) when compared to control (average trace of 171 cells), with a significant reduction of quenching slope in si-TRPM7 cells (histograms; $P<0.001$).

$P<0.05$; Figure 7*F*). Taken together, these results show that TRPM7 regulates the Hsp90α/uPA/MMP-2 proteolytic pathway in PDAC cells.

Role of TRPM7 in Mg^{2+}-entry and PDAC Cell Invasion

Extracellular Mg^{2+} elevation from 1 to 10 mM induces an increase of intracellular MagFura-2 fluorescence from 0.76±0.01 to 0.77±0.01 in control MIA PaCa-2 cells ($n=46$; $P<0.001$ using a Wilcoxon signed rank test; Figure 8, *A* and *B*). On the other hand, TRPM7 silencing abolishes the increase of MagFura-2 fluorescence induced by 10 mM Mg^{2+}, indicating that Mg^{2+} entry is mainly regulated by TRPM7 in MIA PaCa-2 cells ($n=62$; $P>0.05$; Figure 8, *A* and *B*).

Furthermore, we assessed how external Mg^{2+} can regulate PDAC cell invasion and MMP secretion. External Mg^{2+} elevation from 1 to 10 mM increases MIA PaCa-2 cell invasion (165.54±9.53%; $n=40$; $N=2$) when compared to control (100±5.37%; $n=40$; $N=2$; $P<0.001$; Figure 8*C*). TRPM7 silencing decreases cell invasion, but 10 mM external Mg^{2+} is not able to restore cell invasion (70.95±4.38%; $n=40$; $N=2$) when compared to control (54.32±3.43%; $n=40$; $N=2$; $P>0.05$; Figure 8*C*). Finally, pro-MMP-2 secretion was increased (141.31±11.25%; $N=4$) in external media containing 10 mM Mg^{2+} when compared to control media containing 1 mM Mg^{2+} (100±8.48%; $N=4$; $P<0.05$; Figure 8*D*). These results indicate that Mg^{2+} entry through TRPM7 channels is correlated with PDAC cell invasion and MMP secretions.

TRPM7 expression in metastatic lymph node

We have previously shown that TRPM7 is overexpressed in PDAC tissues in correlation with grade and survival [24]. Here, we study the expression of TRPM7 in PDAC and associated lymph nodes metastasis (LNM). We observed that TRPM7 expression in LNM is correlated with TRPM7 expression levels in PDAC primary tumor (Figure 9*A*). Indeed, a low TRPM7 staining in pancreatic tissue is associated to a low TRPM7 staining in lymph node samples (0.27±0.07; $n=14$), whereas a high TRPM7 staining in pancreatic tissue is associated to a higher TRPM7 staining in lymph nodes (1.1±0.16; $n=8$; $P<0.001$; Figure 9*B*). These data show a strong association of the expression levels of TRPM7 in primary tumor and in metastatic PDAC cells that disseminate from the pancreas.

Discussion

In the present study, we show that TRPM7 channels are involved in PDAC cell invasiveness through the regulation of Hsp90α/uPA/MMP-2 proteolytic pathway. The main results of this work are as follows: 1) TRPM7 regulates constitutive cation entry in PDAC cells and mainly in Mg^{2+} homeostasis and influx, 2) TRPM7 promotes basal PDAC cell invasion, 3) TRPM7 is required for Hsp90α secretion leading to uPA and pro-MMP-2 activations and stabilizations, and 4) TRPM7 expression level is maintained from primary tumor to metastatic lymph nodes.

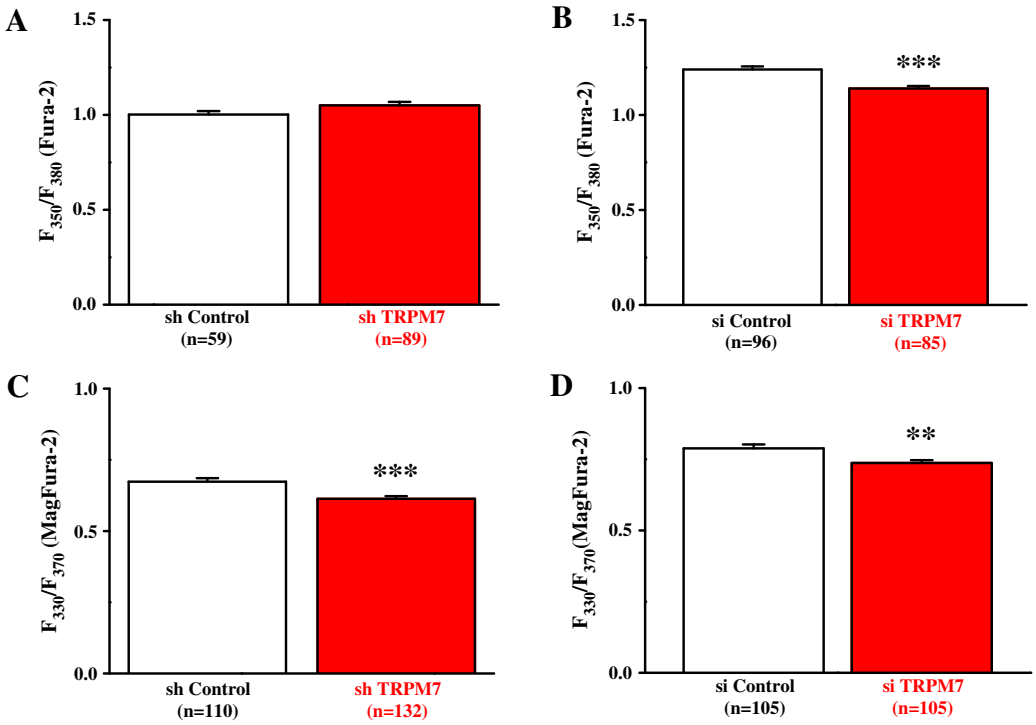

Figure 5. TRPM7 role in basal intracellular Ca^{2+} and Mg^{2+} levels. Ca^{2+} and Mg^{2+} homeostasis was assessed by basal Fura-2 and by MagFura-2 fluorescence ratio, respectively. (A) TRPM7 silencing by shRNA had no effect on PANC-1 basal Ca^{2+} levels ($n=89$ cells) when compared to control ($n=59$ cells; $P>0.05$). (B) Basal Ca^{2+} level is reduced in MIA PaCa-2 cells where TRPM7 has been silenced ($n=85$ cells) when compared to control ($n=96$ cells; $P<0.001$). (C) Basal Mg^{2+} level is reduced by TRPM7 silencing ($n=132$ cells) in PANC-1 when compared to control ($n=110$ cells; $P<0.001$). Basal Mg^{2+} level is also reduced in MIA PaCa-2 cells transfected with si-TRPM7 ($n=105$ cells) when compared to control ($n=105$ cells; $P<0.01$).

We previously showed that TRPM7 is overexpressed in PDAC tissues in correlation with cancer grade and patient survival [24]. We also demonstrated that TRPM7 regulates BxPC-3 cell migration and basal cytosolic Mg^{2+} [24]. However, although BxPC-3 is one of the most commonly used PDAC cell lines, it is probably not representative of the majority of pancreatic cancers [31]. Indeed, BxPC-3 cells contain wild-type RAS, whereas KRAS mutation occurs in almost all PDACs. Then, we assessed the role of TRPM7 in PANC-1 and MIA PaCa-2 PDAC cell lines with mutated KRAS. Moreover, PANC-1 and MIA PaCa-2 cells are more tumorigenic because they produce the largest tumors *in vivo* than BxPC-3 cells [31]. To our knowledge, no relation has been made between mutated KRAS and TRPM7 expression or activity. However, Meng et al. [18] showed that TRPM7 regulates MDA-MB-435 migration and invasion through MAPK pathway. As MAPK pathway is often activated by constitutive KRAS activity in cancer, an interaction between TRPM7 and KRAS could be possible. Further experiments are needed to assess the relation between TRPM7 and KRAS in the regulation of PDAC cell invasion.

Our present work, in accordance with a recent publication from Yee's laboratory [25], confirms that TRPM7 is involved in PDAC progression and PDAC cell ability to migrate and invade. Several studies have reported the involvement of TRPM7 in cell migration and invasion induced by fetal calf serum (FCS) as chemoattractant in breast [18,26], nasopharyngeal [20,21], and pancreatic cancer cells [25]. In our work, it is important to note that we do not use any stimulation (by chemotaxis or activator) to promote cell invasion. Our data strongly indicate that TRPM7 is constitutively active at the plasma membrane of PDAC cells, leading to sustained cation entry and enhanced invasion without any stimulation by chemoattractant or activator. These results are important because they show that TRPM7 is an integral membrane protein that promotes PDAC cell invasiveness independently of external stimuli. However, the molecular mechanisms involved in TRPM7 constitutive activation remain unclear and are still under debate. The MIC current recorded in TRPM7 is inhibited by free intracellular Mg^{2+} within the micromolar range [13,14,32]. In our experiments, we show that TRPM7 current is abolished by 680 and 850 μM free $[Mg^{2+}]_i$ in PANC-1 and BxPC-3 cells [24], respectively. If we assume that cytosolic resting Mg^{2+} levels are in the millimolar range in most cells [33], TRPM7 should be inhibited at physiological cytosolic Mg^{2+} levels. There is evidence that Mg^{2+} homeostasis is altered in cancer [34]. For example, Mg^{2+} deficiency promotes metastasis in a model of mice xenograft [35]. Interestingly, free $[Mg^{2+}]_i$ measurements in human colon carcinoma cells using fluorescent probes show low cytosolic free Mg^{2+} under 0.3 mM [36]. Moreover, a recent study on rat glioma shows that the cancer tissue and the single infiltrating cancer cells contain elevated levels of bound Mg when compared to the noncancer ones [37]. Indeed, elevated bound Mg in cancer may buffer free Mg^{2+}, leading to low intracellular free Mg^{2+} that allows a sustained Mg^{2+} influx through TRPM7. Further experiments on free $[Mg^{2+}]_i$ measurements in PDAC cells are definitely needed to better understand how TRPM7 is constitutively active.

TRPM7 is a Ca^{2+}/Mg^{2+} permeable channel involved in both divalent cation homeostases. In PDAC, we show that TRPM7 silencing affects divalent cation homeostasis in a cell line–dependent manner. Indeed, TRPM7 silencing decreases basal cytosolic Mg^{2+}

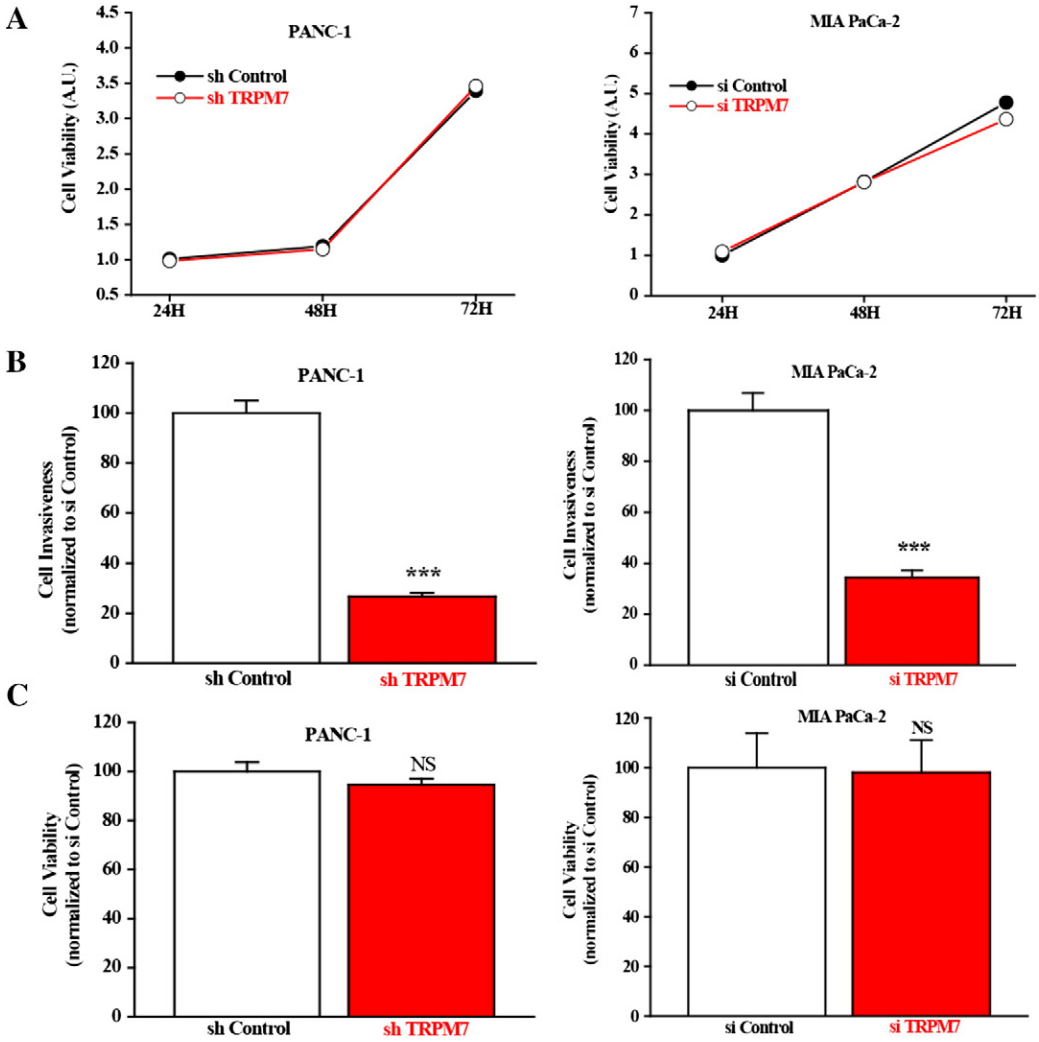

Figure 6. TRPM7 regulated PDAC cell invasiveness. (A) PANC-1 and MIA PaCa-2 cell proliferation was not affected by TRPM7 silencing ($n=12$ counting; $N=3$ for each time tested; $P>0.05$). (B) Both PANC-1 and MIA PaCa-2 cell invasion (40.10^4 cells, 24 hours) assessed in Matrigel modified Boyden chambers was decreased by TRPM7 silencing when compared to control ($n=120$ counting; $N=3$ for PANC-1; $n=100$ counting; $N=3$ for MIA PaCa-2; $P<0.001$ for each PDAC cell line). (C) Cell viability assessed by MTT assays (40.10^4 cells, 24 hours) showed no effect of TRPM7 for PANC-1 cells ($n=12$ counting; $N=3$; $P>0.05$) and for MIA PaCa-2 cells ($n=12$ counting; $N=3$; $P>0.05$).

levels in PANC-1 and MIA PaCa-2 as previously shown in BxPC-3 cells [24]. Moreover, we show that TRPM7 silencing decreases the Mg^{2+} influx induced by the increase of external Mg^{2+}. Taken together, our data strongly indicate that TRPM7 mainly regulates Mg^{2+} homeostasis and influx in PDAC cells.

One of the novelties of our work is that we clearly established a link between TRPM7 expression and a proteolytic pathway in PDAC cells. Indeed, TRPM7 silencing dramatically inhibits Hsp90α secretion and both uPA and pro-MMP-2 secretions in the two cell lines. A recent study showed that inhibiting TRPM7 by siRNA or by pharmacological blocker (carvacol) decreased membrane MMP-2 expression and cell invasion in glioblastoma [17], indicating a regulation of MMP expression by TRPM7. The Hsp90α/uPA/MMP-2 proteolytic pathway is activated by elastin peptides, leading to enhanced cell migration and invasion in fibrosarcoma [38]. There is increased interest in the development of Hsp90 inhibitors for cancer therapy [39,40]. Indeed, aberrant Hsp90α ectopic localization in cancer cells led to cancer progression and enhanced aggressiveness, whereas blocking secreted Hsp90α has an inhibitory effect on metastatic behavior [40]. Moreover, high plasma Hsp90α levels are positively correlated with tumor malignancy in clinical tumor patients [41]. The main biological role of secreted Hsp90α is to interact with MMP-2, leading to protease activation and cancer cell invasiveness [42,43]. Moreover, Hsp90α secretion also activates uPA system [38,44], which is largely involved in cancer metastasis [45]. Indeed, uPA system suppression retards both cell invasion and *in vivo* tumor development in PDAC [46]. How cancer cells constitutively secrete Hsp90α is still largely unknown. To our knowledge, we report, for the first time, that Hsp90α secretion is regulated by TRPM7. However, the molecular mechanisms involved in Hsp90α secretion induced by TRPM7 are still unknown. Several hypotheses are possible due to the dual function of TRPM7. In the present study, we show that TRPM7 induced a constitutive divalent cations entry in PDAC cells. It has been shown that divalent cations such as Mg^{2+} and Ca^{2+} stabilize Hsp90 oligomerization [47]. Furthermore, Hsp90α plasma membrane translocation is regulated by cytosolic Ca^{2+} levels

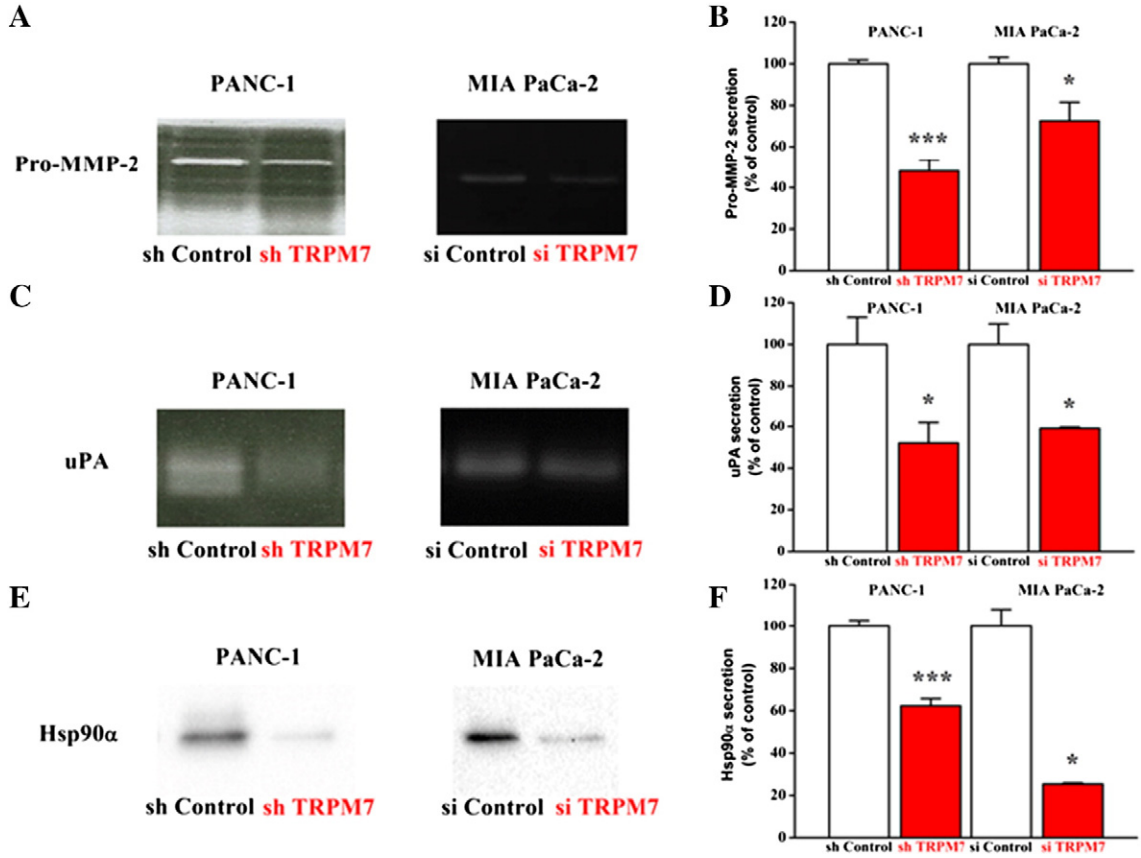

Figure 7. TRPM7 regulates Hsp90α/uPA/MMP-2 pathway in PDAC cells. (A) Typical examples of reduced Pro-MMP-2 secretion following TRPM7 silencing in PANC-1 cells (left panel) and in MIA PaCa-2 cells (right panel). (B) Quantification of decreased pro-MMP-2 secretion induced by TRPM7 silencing in both PANC-1 cells ($N=3$) and MIA PaCa-2 cells ($N=4$). (C) Typical examples of reduced uPA secretion following TRPM7 silencing in PANC-1 cells (left panel) and MIA PaCa-2 cells (right panel). (D). Quantification of decreased uPA secretion induced by TRPM7 silencing in both PANC-1 cells ($N=3$) and MIA PaCa-2 cells ($N=3$). (E) Typical examples of reduced Hsp90α secretion following TRPM7 silencing in PANC-1 cells (left panel) and in MIA PaCa-2 cells (right panel). (F) Quantification of decreased Hsp90α secretion induced by TRPM7 silencing in both PANC-1 cells ($N=3$) and MIA PaCa-2 cells ($N=4$).

[48]. Taken together, these data indicate that Ca^{2+} and Mg^{2+} are important for Hsp90α stabilization and secretion. Thus, it is tempting to speculate that TRPM7 provides a constitutive Ca^{2+}/Mg^{2+} pore leading to Hsp90α secretion. Moreover, one of the posttranslational modifications that promote Hsp90α secretion is phosphorylation on threonine residues [40]. Indeed, Hsp90α phosphorylation by protein kinase A and C on threonine residues leads to its secretion and malignancy [41,49]. In full agreement with these studies, it was shown that TRPM7 kinase domain is required for human breast cancer cell migration [19] and metastasis [26]. Moreover, cytosolic Mg^{2+} has been implicated in the activation of TRPM7 phosphotransferase activity [50,51]. Thus, constitutive Mg^{2+} entry through TRPM7 channel could induce sustained kinase activation, leading to Hsp90α phosphorylation and secretion in PDAC cells. Nevertheless, further studies are needed to determine whether TRPM7 kinase could phosphorylate Hsp90α, leading to secretion and PDAC enhanced cell invasiveness.

From a clinical point of view, our study confirms that TRPM7 could be a promising target in PDAC. It was previously shown that TRPM7 overexpression in PDAC tissues is positively correlated with cancer progression and poor survival [24,25]. Here, we show that high TRPM7 expression is also found in metastatic lymph nodes. Taken together, our work strongly suggests that TRPM7 is required for metastatic dissemination of PDAC cells.

In conclusion, we provide a new molecular mechanism involving TRPM7 in PDAC cell invasiveness. Indeed, TRPM7 activity through Mg^{2+} constitutive entry and possibly kinase activation could lead to Hsp90α secretion inducing MMP-2 and uPA system activations, both enhancing PDAC cell invasiveness (Figure 10).

Materials and Methods

Human pancreatic cancer cell lines PANC-1 (ATCC CRL-1469) and MIA PaCa-2 (ATCC CRL-1420) were used for this study. These cell lines were derived from a poorly differentiated tumor which corresponds to a grade 3 PDAC [31]. PANC-1 and MIA PaCa-2 cells were cultured in Dulbecco's modified Eagle's medium (Gibco) supplemented with 10% FCS (Lonza). Cells were trypsinized once a week using trypsin-EDTA (Sigma-Aldrich) and incubated at +37°C in a humidified atmosphere with 5% CO_2.

TRPM7 Silencing Using siRNA and shRNA

Transient silencing of TRPM7 was performed using siRNA as previously described [24]. Briefly, siRNAs were included in pancreatic cancer cells by nucleofection using a NucleofectorTM II device (Lonza). PANC-1 and MIA PaCa-2 cells (10^6 cells) were transfected with 2 μg of siRNA (corresponding to 1.5 μM) according to the optimized protocol recommended by Lonza. PANC-1 and

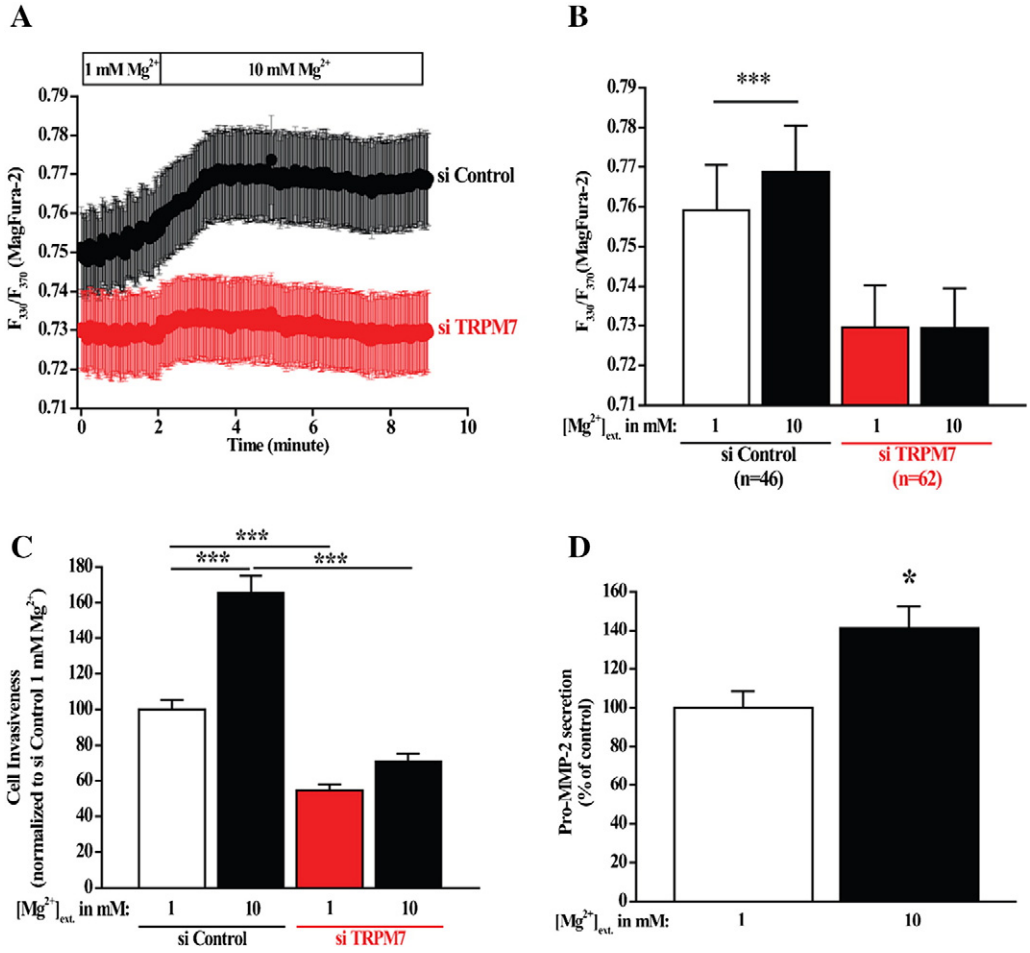

Figure 8. Extracellular Mg^{2+} regulates cell invasion through TRPM7 channels. (A) External application of 10 mM Mg^{2+} at 2 minutes induced a slight but sustained increase of intracellular Mg^{2+} levels in si-Control MIA PaCa-2 (black trace, $n=46$), whereas no effect was observed in si-TRPM7 condition (red trace, $n=62$). (B) Quantification of intracellular MagFura-2 fluorescence following 9-minute application of 10 mM Mg^{2+} in si-Control ($n=46$) and si-TRPM7 MIA PaCa-2 ($n=62$) indicating that TRPM7 mediates Mg^{2+} entry ($P<0.001$ using paired Wilcoxon signed tests). (C) External application of 10 mM Mg^{2+} increases MIA PaCa-2 invasion in si-Control but not in si-TRPM7 condition ($n=40$ counting; $N=2$ passages; $P<0.001$ using two-way analysis of variance followed by Holm-Sidak tests). (D). Pro-MMP-2 secretion is increased by adding 10 mM Mg^{2+} in culture media ($N=4$; $P<0.05$).

MIA PaCa-2 cells were nucleofected with a scrambled siRNA (si-Control) or with a siRNA targeting TRPM7 (si-TRPM7) (targeting nucleotide sequence: 5′-GTC-TTG-CCA-TGA-AA-T-ACT-C-3′). We also used shRNAs for stable and inducible TRPM7 silencing. PANC-1 cells were transfected with shTRPM7 and shControl by nucleofection (10^6 cells with 1 µg plasmid). Cells with shRNAs were selected following puromycin incubation at the concentration of 800 $ng.ml^{-1}$. Stable TRPM7 silencing was induced by doxycycline treatment (2 $\mu g.ml^{-1}$). All si- and shRNAs were purchased from Dharmacon Research Inc., USA.

All the experiments were made in the 48 hours following the nucleofection and in the 72 hours following shRNA induction by doxycycline treatment.

RT-PCR and Quantitative RT-PCR

RNA extraction was performed using the standard Trizol-phenol-chloroform protocol. Total RNA (1 µg) was reverse-transcribed into cDNA with random hexamers and Multi-Scribe Reverse Transcriptase (Applied Biosystems). PCRs were carried out using an iCycler thermal cycler (Biorad) and Taq DNA polymerase (Invitrogen) with, respectively, 30 and 40 cycles for β-actin and TRPM7 primers. PCR products were visualized on agarose gels and quantified using Quantity One Software (Biorad). Results were expressed as TRPM7 expression normalized to β-actin expression for semiquantitative RT-PCR experiments. Quantitative RT-PCR was performed on a LightCycler system (Roche) using a mix containing SYBR green (Applied Biosystem). TRPM7 mRNA quantities were normalized to β-actin as a housekeeping gene.

Western Blotting Experiments

Cells were lysed 30 minutes on ice in radioimmunoprecipitation assay buffer (1% Triton X-100, 1% Na deoxycholate, 150 mM NaCl, 10 mM PO_4Na_2/K, pH 7.2) supplemented with Sigma P8340 inhibitors cocktail, 2 mM EDTA, and 5 mM orthovanadate. After sonication and centrifugation at 13,000 rpm, the proteins in the supernatant were quantified using the BCA method (BioRad). Equal amounts of each protein sample (50 µg) were separated by electrophoresis on sodium dodecyl sulfate (SDS) polyacrylamide gel electrophoresis and blotted onto nitrocellulose membrane (Amersham). Blots were incubated with antibodies raised against TRPM7 (1/1000,

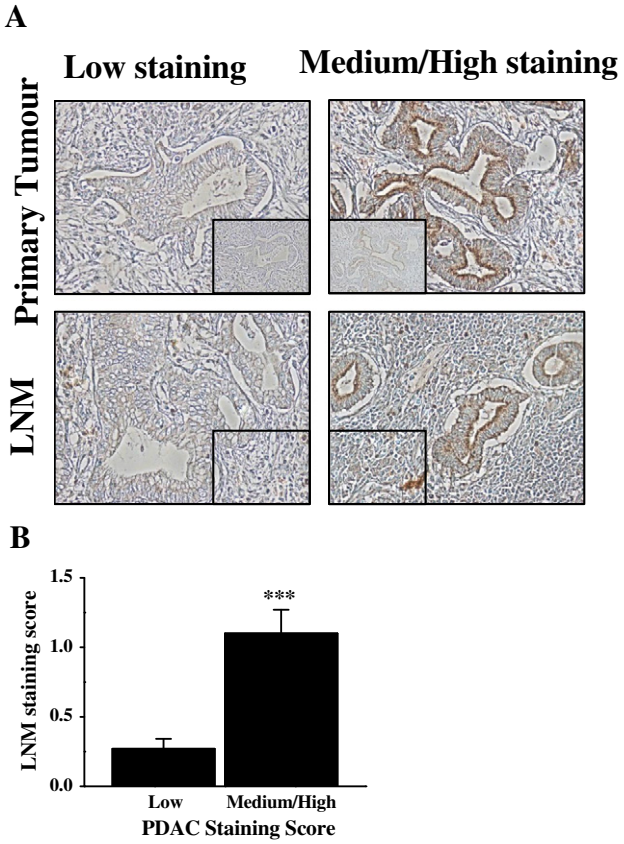

Figure 9. TRPM7 expression in human PDAC and LNM. (A) Examples of low (left panels) and high (right panels) apical and membranous staining in pancreatic (upper panels) and LNM (lower panels) tumor cells using TRPM7 antibody. (Inserts) Negative control obtained by omitting the primary antibody. (B) Correlation between pancreatic ($n=13$) and LNM ($n=22$) staining score for TRPM7 ($P<0.001$).

Abcam) and actin (1/1000, Santa Cruz Biotechnology) and developed with the enhanced chemiluminescence system using specific peroxidase-conjugated anti-IgG secondary antibodies.

Electrophysiology

TRPM7 currents were recorded using the conventional technique of patch clamp in the whole-cell configuration. Holding membrane potential was held to −40 mV, and currents were elicited by a ramp depolarization from −100 mV to +100 mV for 350 milliseconds. Interval between each ramp depolarization was 10 seconds. The patch pipettes (3-5 MΩ) were made from hematocrit glass using a vertical puller (P30 vertical micropipette puller, Sutter Instrument Co.). The extracellular solution was composed of the following (in mM): Na-gluconate 140; K-gluconate 5; Mg-Gluconate 2; Ca-gluconate 2; HEPES 10; glucose 5; TEA-Cl 5 (pH adjusted to 7.4 with NaOH). The intrapipette solution was composed of the following (in mM): Cs-gluconate 145; Na-gluconate 8; EGTA 10; Mg-gluconate or MgATP (as indicated); HEPES 10 (pH adjusted to 7.2 with CsOH). Free $[Mg^{2+}]_i$ was estimated using the program WEBMAXC STANDARD (http://www.stanford.edu/~cpatton/webmaxcS.htm). Signals were filtered at 1 kHz and digitized at 5 kHz using an Axopatch 200B patch clamp amplifier (Molecular Devices Inc.) combined with a 1322A Digidata (Molecular Devices Inc.). The MIC current was recorded after the dialysis of intracellular media by 0 Mg intrapipette solution. The MIC current was calculated as the difference between the steady-state current activated by the depletion of $[Mg^{2+}]_i$ and the basal current recorded few minutes after patch rupture. MIC currents were expressed as current densities (in $pA.pF^{-1}$) by dividing the current intensity (in pA) by the cell capacitance (in pF). Electrophysiological protocols and analyses were made using pClamp 10, Clampfit (both by Molecular Devices), and Origin 6.0 (Microcal Software, Inc.). All experiments were performed at room temperature.

Cell Imaging

PDAC cells were plated on glass coverslips in 35-mm diameter dishes at a density of 8.10^4 cells. After 48 hours, cells were loaded in cell growth medium at +37°C for 1 hour with 3 μM Fura 2-AM (Sigma-Aldrich) or 3 μM Mag-Fura 2-AM (Invitrogen) and subsequently washed three times with the extracellular solution. The coverslip was then transferred onto a perfusion chamber on a Zeiss microscope equipped for fluorescence.

To estimate the divalent cation influx, we used Mn^{2+} quenching as previously published [24]. Cells were perfused for 1 minute with extracellular solution containing (in mM) 145 NaCl, 5 KCl, 2 $CaCl_2$, 1 $MgCl_2$, 10 HEPES, and 5 glucose (pH adjusted to 7.4 with NaOH). After this period, Ca^{2+} was replaced by Mn^{2+} (2 mM). To measure Mn^{2+} influx, cells were excited at 360 nm with a monochromator (TILLVR Photonics, Munich, Germany), and fluorescence emission was monitored at 510 nm by a CCD camera coupled to a Zeiss inverted microscope (Carl Zeiss MicroImaging, LLC, Oberkochen, Germany). After Mn^{2+} perfusion, the decrease of Fura-2 fluorescence described a linear decay, and the slope is correlated with the rate of the Mn^{2+} influx. The calculated slope is obtained by subtracting the slope of basal decreasing Fura-2 fluorescence obtained in basal conditions (culture conditions) and after Mn^{2+} application. To measure the Ca^{2+} basal fluorescence ratio, PANC-1 and MIA PaCa-2 were incubated with Fura-2AM as previously indicated. Cells were then perfused with the extracellular solution containing 2 mM of Ca^{2+}. Cells were excited alternatively at 350 nm and 380 nm. The fluorescence emission was monitored at 510 nm. The ratio of Fura-2 fluorescence intensities measured with excitation at 350 and 380 nm (F_{350}/F_{380}) was used as a $[Ca^{2+}]_i$-related signal. The same protocol was used for Mg^{2+} basal ratio, but cells were perfused by extracellular solution which contained 1 mM Mg^{2+}, and MAG-Fura-2AM was used as a fluoroprobe. The ratio of MAG-Fura-2 fluorescence intensities measured with excitation at 330 and 370 nm (F_{330}/F_{370}) was used as a $[Mg^{2+}]_i$-related signal.

Cell Migration and Invasion Assays

Migration tests were performed in 8-μm pore size polyethylene terephthalate membrane cell culture inserts (BD FALCON Cell Culture Inserts, BD Biosciences). The upper compartment was seeded with 4×10^4 cells of 24-hour transfected PANC-1 cells (scramble or siTRPM7) in growth medium supplemented with 10% FCS. The lower compartment was also filled with growth medium supplemented with 10% FCS. Thus, migration and invasion assays were performed without addition of chemoattractant. After 24 hours of further incubation at 37°C, the remaining cells were removed from the upper side of the membrane by scrubbing. Migrated cells on the lower side were washed by phosphate-buffered saline, fixed by methanol, and stained by hematoxylin. Migrated cells were counted

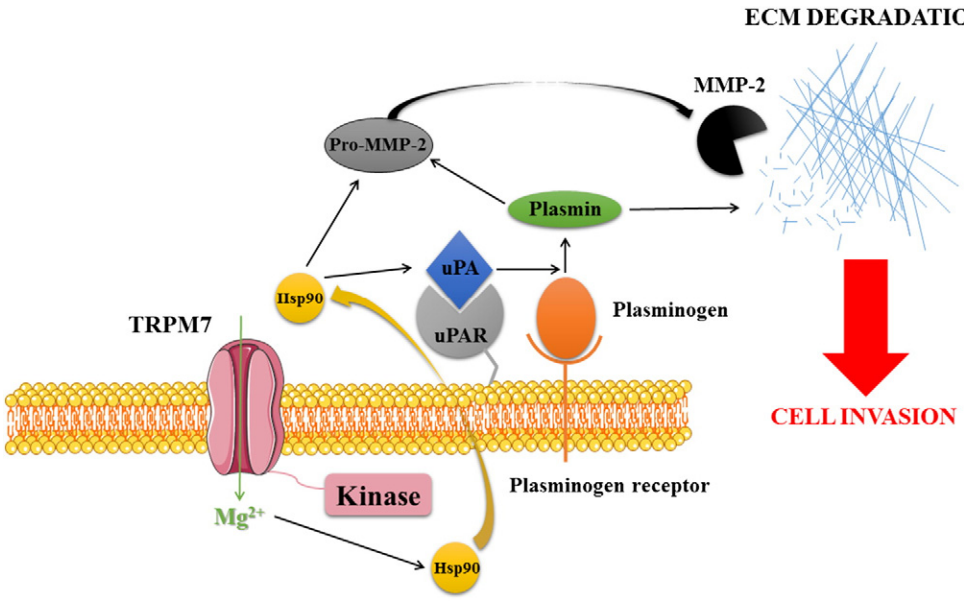

Figure 10. Graphical conclusion. TRPM7 is involved in basal Mg^{2+} influx in PDAC cells and secretion of Hsp90α. Hsp90α stabilizes both pro-MMP-2 and uPA/plasmin pathway that in turn enhances extracellular matrix (ECM) degradation and PDAC cell invasiveness.

under an inverted microscope (Zeiss) in duplicate (20 contiguous areas at ×400 magnification for each insert). For each experiment, the number of migrating cells per area for each condition (scramble or siTRPM7) was normalized by the mean of scramble migrating cells. Experiments were repeated in three different passages. For each passage, an MTT test was carried out in the same condition as the migration assays (24 hours after cell nucleofection). Invasion assays were made in the same manner as that for migration. The upper side of the migration inserts was coated with Matrigel.

Proteinase and Hsp90 Detection

Conditioned media from PANC-1 and MIA PaCa-2 cell cultures were analyzed for gelatin degradation by electrophoresis under nonreducing conditions on an SDS-polyacrylamide gel containing 1 mg/ml of gelatin with or without 3 μg/ml of plasminogen. The volume of conditioned medium loaded per lane was standardized on the basis of the cell count at harvest. Following electrophoresis, gels were incubated overnight at +37°C in 50 mM Tris-HCl, 150 mM NaCl, and 10 mM $CaCl_2$, pH 7.4, for matrix metalloproteinase detection and 100 mM glycine buffer and EDTA 5 mM, pH 8.3, for plasminogen activator detection. Gelatinolytic activity resulting from proteinase presence was indicated here by white lysis zones which were revealed by staining with Coomassie brilliant blue. As a positive control, HT-1080 conditioned medium was used.

To detect secreted Hsp90, conditioned media were concentrated in Vivaspin from Sartorius stedim (Aubagne, France), and samples were electrophoresed in a 0.1% SDS, 10% polyacrylamide gel, under reducing conditions. Proteins were then transferred onto Immobilon-P membrane (Millipore, Saint-Quentin en Yvelines, France). The membrane was blocked with 5% nonfat dry milk, 0.1% Tween 20 in a 50-mM Tris-HCl buffer, 150 mM NaCl, pH 7.5 (TBS), for 2 hours at room temperature and incubated overnight at +4°C with anti-Hsp90 antibody (Ozyme, Saint Quentin Yvelines, France) and then for 1 hour at room temperature with a second peroxidase-conjugated anti-IgG antibody. Immune complexes were visualized with the enhanced chemoluminescence detection kit (GE Healthcare, Orsay, France).

TRPM7 Detection in PDAC and Associated Lymph Nodes

Human tissues samples from PDAC (n=13) including LNM (n=22) were used with the agreement of patients treated by surgery in the University Hospital of Amiens (Picardie, France). Experiments on human tissues were approved by the Comité Consultatif de Protection des Personnes dans la Recherche Biomédicale de Picardie (Amiens, France). Histological examination was performed by an experimented pathologist (D.C.) on paraffin-embedded tissues using hematoxylin-phloxin-saffron staining.

Immunohistochemistry was performed in duplicate for each sample using the indirect immunoperoxidase staining technique on the paraffin-embedded material with a Ventana XT instrument (Ventana Medical Systems, Roche Diagnostics) and a hematoxylin counterstain as previously described [24]. The sections were incubated with anti-TRPM7 antibody (Chemicon, 1/300), and negative controls were performed by omitting the primary antibodies. Analysis of tissue section was done by light microscopy by a pathologist (D.C.) at ×400 magnification. Because PDAC tissues showed a nonhomogenous staining, TRPM7 staining in human PDAC was determined by the previously published method [52]. Briefly, the percentages of tumor cells (in well differentiated and undifferentiated areas) that were stained at each of the intensity score 0 (no staining), 1 (weak staining), 2 (moderate staining), and 3 (strong staining) were added, and the sum of these scores gave a final score for each tissue ranging from 0 to 0.99 (weak TRPM7 staining), 1 to 1.99 (moderate TRPM7 staining), or 2 to 2.99 (strong TRPM7 staining).

Statistical Analysis

Data are presented as mean±SEM, n refers to the number of separate experiments or to the number of cells, and N refers to the number of cell line passages. Statistical analyses were made using Student's t tests or Mann-Whitney rank sum test depending on sample normality or paired Wilcoxon signed rank test using Sigma-Stat 3.0 (Systat Software, Inc.).

When more than two conditions were compared, a Kruskal-Wallis one-way analysis of variance was used followed by Dunn's method *post hoc* tests using SigmaStat 3.0 (Systat Software, Inc.).

Funding

P. R. was a recipient of funding from the Ministère de l'Enseignement Supérieur et de la Recherche. A. V. is a recipient of funding from the Conseil Régional de Picardie. This work was supported by FEDER, la Ligue Contre le Cancer (Septentrion), and la SFR CAP-Santé (FED 4231).

Conflict of Interest Statement

None.

Acknowledgements

The authors thank Aurélie Dupont-Deshorgue and Marie-Pierre Mabille for their technical help.

Appendix A. Supplementary data

Supplementary data to this article can be found online at http://dx.doi.org/10.1016/j.neo.2017.01.004.

References

[1] Hariharan D, Saied A, and Kocher HM (2008). Analysis of mortality rates for pancreatic cancer across the world. *HPB (Oxford)* **10**, 58–62.
[2] Stathis A and Moore MJ (2010). Advanced pancreatic carcinoma: current treatment and future challenges. *Nat Rev Clin Oncol* **7**, 163–172.
[3] Prevarskaya N, Skryma R, and Shuba Y (2011). Calcium in tumour metastasis: new roles for known actors. *Nat Rev Cancer* **11**, 609–618.
[4] Stock C and Schwab A (2015). Ion channels and transporters in metastasis. *Biochim Biophys Acta* **1848**, 2638–2646.
[5] Huang X and Jan LY (2014). Targeting potassium channels in cancer. *J Cell Biol* **206**, 151–162.
[6] Ouadid-Ahidouch H, Ahidouch A, and Pardo LA (2016). Kv10.1K(+) channel: from physiology to cancer. *Pflugers Archiv* **468**, 751–762.
[7] Pardo LA and Stuhmer W (2014). The roles of K(+) channels in cancer. *Nat Rev Cancer* **14**, 39–48.
[8] Stewart TA, Yapa KT, and Monteith GR (2015). Altered calcium signaling in cancer cells. *Biochim Biophys Acta* **1848**, 2502–2511.
[9] Vashisht A, Trebak M, and Motiani RK (2015). STIM and Orai proteins as novel targets for cancer therapy. A Review in the Theme: Cell and Molecular Processes in Cancer Metastasis. *Am J Physiol Cell Physiol* **309**, C457–C469.
[10] Prevarskaya N, Ouadid-Ahidouch H, Skryma R, and Shuba Y (2014). Remodelling of Ca2+ transport in cancer: how it contributes to cancer hallmarks? *Philos Trans R Soc Lond B Biol Sci* **369**, 20130097.
[11] Besson P, Driffort V, Bon E, Gradek F, Chevalier S, and Roger S (2015). How do voltage-gated sodium channels enhance migration and invasiveness in cancer cells? *Biochim Biophys Acta* **1848**, 2493–2501.
[12] Fraser SP, Ozerlat-Gunduz I, Brackenbury WJ, Fitzgerald EM, Campbell TM, Coombes RC, and Djamgoz MB (2014). Regulation of voltage-gated sodium channel expression in cancer: hormones, growth factors and auto-regulation. *Philos Trans R Soc Lond B Biol Sci* **369**, 20130105.
[13] Nadler MJ, Hermosura MC, Inabe K, Perraud AL, Zhu Q, Stokes AJ, Kurosaki T, Kinet JP, Penner R, and Scharenberg AM, et al (2001). LTRPC7 is a Mg.ATP-regulated divalent cation channel required for cell viability. *Nature* **411**, 590–595.
[14] Runnels LW, Yue L, and Clapham DE (2001). TRP-PLIK, a bifunctional protein with kinase and ion channel activities. *Science* **291**, 1043–1047.
[15] Visser D, Langeslag M, Kedziora KM, Klarenbeek J, Kamermans A, Horgen FD, Fleig A, van Leeuwen FN, and Jalink K (2013). TRPM7 triggers Ca2+ sparks and invadosome formation in neuroblastoma cells. *Cell Calcium* **54**, 404–415.
[16] Clark K, Langeslag M, van Leeuwen B, Ran L, Ryazanov AG, Figdor CG, Moolenaar WH, Jalink K, and van Leeuwen FN (2006). TRPM7, a novel regulator of actomyosin contractility and cell adhesion. *EMBO J* **25**, 290–301.
[17] Chen WL, Barszczyk A, Turlova E, Deurloo M, Liu B, Yang BB, Rutka JT, Feng ZP, and Sun HS (2015). Inhibition of TRPM7 by carvacrol suppresses glioblastoma cell proliferation, migration and invasion. *Oncotarget* **6**, 16321–16340.
[18] Meng X, Cai C, Wu J, Cai S, Ye C, Chen H, Yang Z, Zeng H, Shen Q, and Zou F (2013). TRPM7 mediates breast cancer cell migration and invasion through the MAPK pathway. *Cancer Lett* **333**, 96–102.
[19] Guilbert A, Gautier M, Dhennin-Duthille I, Rybarczyk P, Sahni J, Sevestre H, Scharenberg AM, and Ouadid-Ahidouch H (2013). Transient receptor potential melastatin 7 is involved in oestrogen receptor–negative metastatic breast cancer cells migration through its kinase domain. *Eur J Cancer* **49**, 3694–3707.
[20] Chen JP, Luan Y, You CX, Chen XH, Luo RC, and Li R (2010). TRPM7 regulates the migration of human nasopharyngeal carcinoma cell by mediating Ca(2+) influx. *Cell Calcium* **47**, 425–432.
[21] Chen JP, Wang J, Luan Y, Wang CX, Li WH, Zhang JB, Sha D, Shen R, Cui YG, and Zhang Z, et al (2015). TRPM7 promotes the metastatic process in human nasopharyngeal carcinoma. *Cancer Lett* **356**, 483–490.
[22] Gao H, Chen X, Du X, Guan B, Liu Y, and Zhang H (2011). EGF enhances the migration of cancer cells by up-regulation of TRPM7. *Cell Calcium* **50**, 559–568.
[23] Sun Y, Sukumaran P, Varma A, Derry S, Sahmoun AE, and Singh BB (2014). Cholesterol-induced activation of TRPM7 regulates cell proliferation, migration, and viability of human prostate cells. *Biochim Biophys Acta* **1843**, 1839–1850.
[24] Rybarczyk P, Gautier M, Hague F, Dhennin-Duthille I, Chatelain D, Kerr-Conte J, Pattou F, Regimbeau JM, Sevestre H, and Ouadid-Ahidouch H (2012). Transient receptor potential melastatin-related 7 channel is over-expressed in human pancreatic ductal adenocarcinomas and regulates human pancreatic cancer cell migration. *Int J Cancer* **131**, E851-861.
[25] Yee NS, Kazi AA, Li Q, Yang Z, Berg A, and Yee RK (2015). Aberrant over-expression of TRPM7 ion channels in pancreatic cancer: required for cancer cell invasion and implicated in tumor growth and metastasis. *Biol Open* **4**, 507–514.
[26] Middelbeek J, Kuipers AJ, Henneman L, Visser D, Eidhof I, van Horssen R, Wieringa B, Canisius SV, Zwart W, and Wessels LF, et al (2012). TRPM7 is required for breast tumor cell metastasis. *Cancer Res* **72**, 4250–4261.
[27] Middelbeek J, Visser D, Henneman L, Kamermans A, Kuipers AJ, Hoogerbrugge PM, Jalink K, and van Leeuwen FN (2015). TRPM7 maintains progenitor-like features of neuroblastoma cells: implications for metastasis formation. *Oncotarget* **6**, 8760–8776.
[28] Guilbert A, Gautier M, Dhennin-Duthille I, Haren N, Sevestre H, and Ouadid-Ahidouch H (2009). Evidence that TRPM7 is required for breast cancer cell proliferation. *Am J Physiol Cell Physiol* **297**, C493–C502.
[29] Mederos y Schnitzler M, Waring J, Gudermann T, and Chubanov V (2008). Evolutionary determinants of divergent calcium selectivity of TRPM channels. *FASEB J* **22**, 1540–1551.
[30] Schmitz C, Perraud AL, Johnson CO, Inabe K, Smith MK, Penner R, Kurosaki T, Fleig A, and Scharenberg AM (2003). Regulation of vertebrate cellular Mg2+ homeostasis by TRPM7. *Cell* **114**, 191–200.
[31] Deer EL, Gonzalez-Hernandez J, Coursen JD, Shea JE, Ngatia J, Scaife CL, Firpo MA, and Mulvihill SJ (2010). Phenotype and genotype of pancreatic cancer cell lines. *Pancreas* **39**, 425–435.
[32] Chokshi R, Matsushita M, and Kozak JA (2012). Sensitivity of TRPM7 channels to Mg2+ characterized in cell-free patches of Jurkat T lymphocytes. *Am J Physiol Cell Physiol* **302**, C1642–C1651.
[33] de Baaij JH, Hoenderop JG, and Bindels RJ (2015). Magnesium in man: implications for health and disease. *Physiol Rev* **95**, 1–46.
[34] Trapani V, Arduini D, Cittadini A, and Wolf FI (2013). From magnesium to magnesium transporters in cancer: TRPM7, a novel signature in tumour development. *Magnes Res* **26**, 149–155.
[35] Nasulewicz A, Wietrzyk J, Wolf FI, Dzimira S, Madej J, Maier JA, Rayssiguier Y, Mazur A, and Opolski A (2004). Magnesium deficiency inhibits primary tumor growth but favors metastasis in mice. *Biochim Biophys Acta* **1739**, 26–32.
[36] Castiglioni S, Cazzaniga A, Trapani V, Cappadone C, Farruggia G, Merolle L, Wolf FI, Iotti S, and Maier JA (2015). Magnesium homeostasis in colon carcinoma LoVo cells sensitive or resistant to doxorubicin. *Sci Rep* **5**, 16538.
[37] Chandra S, Parker DJ, Barth RF, and Pannullo SC (2016). Quantitative imaging of magnesium distribution at single-cell resolution in brain tumors and infiltrating tumor cells with secondary ion mass spectrometry (SIMS). *J Neurooncol* **127**, 33–41.
[38] Donet M, Brassart-Pasco S, Salesse S, Maquart FX, and Brassart B (2014). Elastin peptides regulate HT-1080 fibrosarcoma cell migration and invasion through an Hsp90-dependent mechanism. *Br J Cancer* **111**, 139–148.
[39] Mahalingam D, Swords R, Carew JS, Nawrocki ST, Bhalla K, and Giles FJ (2009). Targeting HSP90 for cancer therapy. *Br J Cancer* **100**, 1523–1529.
[40] Barrott JJ and Haystead TA (2013). Hsp90, an unlikely ally in the war on cancer. *FEBS J* **280**, 1381–1396.

[41] Wang X, Song X, Zhuo W, Fu Y, Shi H, Liang Y, Tong M, Chang G, and Luo Y (2009). The regulatory mechanism of Hsp90alpha secretion and its function in tumor malignancy. *Proc Natl Acad Sci U S A* **106**, 21288–21293.

[42] Eustace BK, Sakurai T, Stewart JK, Yimlamai D, Unger C, Zehetmeier C, Lain B, Torella C, Henning SW, and Beste G, et al (2004). Functional proteomic screens reveal an essential extracellular role for hsp90 alpha in cancer cell invasiveness. *Nat Cell Biol* **6**, 507–514.

[43] Sims JD, McCready J, and Jay DG (2011). Extracellular heat shock protein (Hsp)70 and Hsp90alpha assist in matrix metalloproteinase-2 activation and breast cancer cell migration and invasion. *PLoS One* **6**, e18848.

[44] McCready J, Sims JD, Chan D, and Jay DG (2010). Secretion of extracellular hsp90alpha via exosomes increases cancer cell motility: a role for plasminogen activation. *BMC Cancer* **10**, 294.

[45] Andreasen PA, Kjoller L, Christensen L, and Duffy MJ (1997). The urokinase-type plasminogen activator system in cancer metastasis: a review. *Int J Cancer* **72**, 1–22.

[46] Gorantla B, Asuthkar S, Rao JS, Patel J, and Gondi CS (2011). Suppression of the uPAR-uPA system retards angiogenesis, invasion, and in vivo tumor development in pancreatic cancer cells. *Mol Cancer Res* **9**, 377–389.

[47] Garnier C, Barbier P, Devred F, Rivas G, and Peyrot V (2002). Hydrodynamic properties and quaternary structure of the 90 kDa heat-shock protein: effects of divalent cations. *Biochemistry* **41**, 11770–11778.

[48] Yang J, Song X, Chen Y, Lu XA, Fu Y, and Luo Y (2014). PLCgamma1-PKCgamma signaling-mediated Hsp90alpha plasma membrane translocation facilitates tumor metastasis. *Traffic* **15**, 861–878.

[49] Lu XA, Wang X, Zhuo W, Jia L, Jiang Y, Fu Y, and Luo Y (2014). The regulatory mechanism of a client kinase controlling its own release from Hsp90 chaperone machinery through phosphorylation. *Biochem J* **457**, 171–183.

[50] Matsushita M, Kozak JA, Shimizu Y, McLachlin DT, Yamaguchi H, Wei FY, Tomizawa K, Matsui H, Chait BT, and Cahalan MD, et al (2005). Channel function is dissociated from the intrinsic kinase activity and autophosphorylation of TRPM7/ChaK1. *J Biol Chem* **280**, 20793–20803.

[51] Ryazanova LV, Dorovkov MV, Ansari A, and Ryazanov AG (2004). Characterization of the protein kinase activity of TRPM7/ChaK1, a protein kinase fused to the transient receptor potential ion channel. *J Biol Chem* **279**, 3708–3716.

[52] Ottaviano AJ, Sun L, Ananthanarayanan V, and Munshi HG (2006). Extracellular matrix-mediated membrane-type 1 matrix metalloproteinase expression in pancreatic ductal cells is regulated by transforming growth factor-beta1. *Cancer Res* **66**, 7032–7040.